Autonomic Neuroscience: Basic and Clinical 146 (2009) 62–69

Contents lists available at ScienceDirect

Autonomic Neuroscience: Basic and Clinical

journal homepage: www.elsevier.com/locate/autneu

Does well-harmonized homeostasis exist in heart rate fluctuations? Time series analysis and model simulations

Yuo-Hsien Shiau

Graduate Institute of Applied Physics, National Chengchi University, Taipei 11605, Taiwan, Republic of China

ARTICLE INFO

Article history:
Received 11 March 2008
Received in revised form 3 October 2008
Accepted 24 November 2008

Keywords:
Heart
Time series
Homeostasis
Mathematical models
Diagnosis

ABSTRACT

Analyzing heart rate variability from electrocardiographic recordings has been an important method for assessing cardiovascular autonomic regulation. Researchers have conducted extensive analyses on normal as well as pathological hearts, however, it is still unclear whether increasing or decreasing the complexity of heart rate variability is a characteristic of healthy systems. In this study, we find the existence of well-harmonized homeostasis in heart rate fluctuations, in particular, the evidence is verified among different individuals including healthy subjects, ICU patients, and one child with brainstem dysfunction. The methodology we used is composed of two parts, in which one is the consideration of reduction of cardiorespiratory fluctuations inherited in the original R–R intervals and the other is based upon the concept of nonlinear dynamics to construct the low-dimensional trajectory in the angle plot. The cross-correlation measure between the theoretical angle map and the numerically derived angle trajectory is used to separate recovery (0.73±0.13) from deterioration (0.25±0.08) of ICU patients. In addition, a simple physiologic (deterministic) model of the interaction between the cardiovascular system and baroreceptor control of arterial pressure is used to explain why homeostasis can exist in heart rate fluctuations. Our study provides a potential link between the clinical data and circulatory system.

1. Introduction

It is known that both an epilepsy seizure and a heart attack may be considered as dynamic diseases used to describe diseases highlighted by a change in normal body rhythms. What are normal body rhythms? Conceptually, they are a healthy body's simple rhythms. From this point of view, the different body parts will tend towards homeostasis, and the interrelated systems reach a balance or have simple occasional behavior. Nevertheless, researchers suggested that chaos is the natural way to join different situations in the body. Goldberger et al. (1994) have conducted an extensive analysis of normal and pathological hearts, and claim that chaos provides the body with the flexibility to respond to different stimuli. Thus, healthy systems want to exhibit chaotic/complicated fluctuations. More recently, Andrés et al. (2006) provided a study on cardiac dynamics, and they found that the existence of premature ventricular contraction increases the embedding dimension of heart rate variability (HRV). In addition, patients with congestive heart failure also show an increase in the embedding dimension of HRV. Therefore, it is still unclear whether increasing or decreasing the complexity of HRV is a characteristic of healthy systems.

Analyzing HRV from electrocardiographic (ECG) recordings has been an important method for assessing cardiovascular autonomic regulation (Task Force of the European Society of Cardiology and the North American Society of Pacing and Electrophysiology, 1996). The most commonly used prognostic HRV index has been the standard deviation in N–N intervals (SDNN; one of linear methods), which is analyzed over a 24-h period for risk stratification. Spectral analysis of HRV allows assessment of frequency-specific fluctuations in heart rate and provides prognostic information beyond the SDNN measure. Although all the measures of HRV differ in their manner of computation and analysis, these methods are fundamentally based on moment statistics and describe the magnitude of HRV. It is therefore not surprising that SDNN and spectral analysis all have a relatively close mutual correlation, and that there are only minor differences in prognostic power between them. More recently, nonlinear dynamics has opened new approaches for studying and understanding the characteristics of heart rate (Goldberger, 1996). These methods differ from the above-mentioned measures of HRV in that they are not designed to assess the magnitude of variability. Rather, they estimate the correlation properties and complexity of HRV and other features in heart rate dynamics that are not uncovered by methods based on variance and mean. One of typical nonlinear measures is Poincaré plot analysis that allows visual and quantitative analysis of instantaneous and continuous R–R interval variability and also provides more powerful prognostic information on patients with heart failure and on arrhythmic risk (Huikuri et al., 1996).

In the clinical data, it is known that sinus rhythm in very sick patients often varies in a regular way that appears much simpler

E-mail address: yhshiau@nccu.edu.tw.

1566-0702/$ – see front matter © 2008 Elsevier B.V. All rights reserved.
doi:10.1016/j.autneu.2008.11.017

in form than the variability observed in normal, healthy individuals (Goldberger et al., 1990). Besides, deterministic homoclinic orbits illustrated in the Poincaré plot can be directly observed from symptomatic sinus node dysfunction (Bergfeldt and Haga, 2003). Nevertheless, Kantz and Schreiber (1998) concluded that there is no clear evidence for determinism in R–R intervals. Therefore, the conservative working hypothesis would be that the process which governs the initiation of new cardiac cycles is effectively stochastic, superimposed by the regulations of autonomic nervous system.

Recently, studies were made to create either deterministic or stochastic models describing the behavior of R–R intervals based on the understanding of the physiological mechanisms underlying their variations (Rosenblum and Kurths, 1995; Seidel and Herzel, 1998; Ivanov et al., 1998). Suder et al. (1998) paid their attention on the evolution of angular component of the R–R interval map in humans undergoing paced respiration at a frequency close to 0.1 Hz, and the deterministic structure was found in the angle map. Their point of view is that the complexity of spontaneous respiratory movements obviously precludes the identification of finite dimensional attractors in heart rate fluctuations within the frequency range of breathing, i.e., so-called respiratory sinus arrhythmia (RSA). Therefore, one way to overcome this problem is to introduce paced breathing. The main result of their paper is that HRV during voluntarily induced slow-paced breathing obeys a one-dimensional, nonlinear law of motion. In addition, the one-dimensional law of motion breaks down for cycle lengths close to that of spontaneous breathing. More recently, Balocchi et al. (2004) derived/studied RSA from the heartbeat time series using empirical mode decomposition. In their study, the spontaneous respiratory signal (i.e., respirogram) was recorded simultaneously with ECG, in which they found the existence of phase and frequency synchronization between the R–R intervals associated breathing and the respiratory signal itself. Moreover, it can be verified that the phase distribution of the respiratory signal displays a noise-like homogeneous profile in a range from $-\pi$ to π (Wu et al., 2006). According to these findings, it could be hypothesized that RSA fluctuations include a noisy part which is from the condition of spontaneous breathing.

In the present study, we report the existence of well-harmonized homeostasis in heart rate fluctuations, in particular, the evidence is verified among different individuals including healthy subjects, ICU patients, and one child with brainstem dysfunction. Our analyzing method is a nonlinear measure which allows visual and quantitative analyses of instantaneous and continuous R–R interval variability. Basically, our calculations are based upon the traditional concept of fluctuations in nature, in which a mixture of deterministic and stochastic factors should be considered. In order to extract the deterministic factor embedded in R–R intervals, a noise-reduction method is used to find the *final* as well as *deterministic* R–R intervals displaying a one-dimensional and well-harmonized nonlinear angle map derived from the Poincaré plot, in which the so-called homeostasis can be realized. In this study, we also provide a clinical research on risk stratification for ICU patients in terms of the angle plot. Surprisingly, the outcome of analyzed 25 patients is well described by the present method. Moreover, a simple physiologic (deterministic) model of the interaction between the cardiovascular system and baroreceptor control of arterial pressure is used to explain the status of ICU patients, which could be the result from the influence of time delay in the human baroreceptor-mediated reflex. Thus, our study provides a potential link between the clinical data and the circulatory system.

The remainder of this paper is organized as follows. Subjects and methods are given in Section 2. Section 3 contains the central part of our paper including analyzing the clinical data, surrogate data analysis, and model simulations. Discussions and concluding remarks are given in Sections 4 and 5, respectively.

2. Subjects and methods

2.1. Subjects

A group of 25 healthy normal subjects were recruited/recorded in the Taipei Veterans General Hospital, where sex (10 females and 15 males), age (30±1 years), and body mass index (21.5±0.4 kg/m^2). And 25 patients with diseases including those requiring admission to intensive care unit such as myocardial infarction, multiple organ dysfunction syndrome, sepsis, and heart failure were recruited in this study. The study protocol was approved by the local ethics committee and all participants gave their informed consent. The study was conducted according to the principles of the Helsinki declaration.

2.2. Study protocol

For all healthy normal subjects, no alcoholic or caffeine-containing drinks were taken for at least 24 h before the study. The examination was performed in a quiet room during the daytime. Subjects received ECG measurement in the supine position after five min rest. During the ECG measurement, subjects were instructed to fully relax, stay awake, and not to speak.

2.3. Data acquirement

The raw R–R intervals were deduced from the adjacent normal sinus beats, which were then transferred to a personal computer and post-processed by a program. The missing intervals (due to extra-systoles) were linearly interpolated and the resulting R–R intervals were resampled at 4 Hz by the Berger method (Berger et al., 1986). All analyzed data were checked by a qualified medical doctor. Therefore, possible artifacts appeared in R–R intervals were deleted.

2.4. Nonlinear noise reduction

Suppose we have a scalar time series $\{x_i\}$, $i=1,\ldots,T$, where the x_i are composed of a clean signal y_i with some noise w_i added, $x_i=y_i+w_i$. The $<w^2>$ is called the absolute noise level. The reduction scheme is to replace each noisy x_i by the average value of this coordinate over points in a suitably chosen neighborhood. The neighborhoods are defined in a phase space reconstructed by delay coordinates. In order to define the neighborhoods, one has to fix positive integers k and l and construct embedding vectors $\boldsymbol{x}^i=(x_{i-k},\ldots, x_{i+l})$ as usual. Note that past and future coordinates are involved. Further, choose a radius r for the neighborhoods. For each value x_i find the set $\boldsymbol{U}_i^r$ of all neighbors x_j for which $||\boldsymbol{x}_j-\boldsymbol{x}_i||_{\sup}<r$, i.e., all segments of the trajectory which are close during a time lasting from k iterations in the past to l iterations in the future. Then, replace the "present" coordinate x_i by its mean value in $\boldsymbol{U}_i^r$,

$$x_i^{\mathrm{corr}} = \frac{1}{|U_i^r|}\sum_{U_i^r} x_j. \tag{1}$$

The implementation of the algorithm is straightforward. To obtain optimal results it is essential to choose r, the size of the neighborhoods, appropriately. In addition, the procedure can be iterated. If one takes the rms of the correction made as a new value for r, r will decrease exponentially with the number of iterations until eventually no neighbors are found for any point and no further correction is made (Schreiber, 1993).

To estimate the embedding dimension d for the reconstruction of the phase space, the false nearest neighbor method proposed by Kennel et al. (1992) is used to determine the lower bound of the embedding dimension d_l (Hegger and Kantz, 1999). The d_l value for different individuals, including healthy subjects and ICU patients, is

within the range $7 \le d_l \le 15$. Thus, in the present study we choose $d=21$ (i.e., $l=10$ and $k=10$) as the embedding dimension, which is large enough to reconstruct the phase space for all analyzed subjects. In addition, the initial r values we used are 50 ms.

2.5. Angle map

A first attempt at identifying the underlying process generating the characteristic pattern of HRV is to plot the same data as a two-dimensional scatter (Poincaré) plot of successive R–R intervals. However, no sharply defined pattern is revealed in this plot; the points scatter around an elliptical structure. All R–R intervals of healthy subjects contain this feature, but they do not show a simple nonrandom structure. The elliptical structure reflects the long-term periodicity of R–R intervals under the control of the autonomic nervous system.

As a next step, we focus on the angular motion of the points in the scatter plot. This is done by introducing polar coordinates and by neglecting the fluctuations of the radii. The transformation needs the definition of a center. The center is defined as the mean values of R–R intervals (RR_a). For every pair of successive R–R intervals, an angle ϕ is calculated. The angles are defined to vary between $-\pi$ to π.

$$\phi_n = \arctan\left(\frac{RR_{n+1}-RR_a}{RR_n-RR_a}\right) \tag{2}$$

where ϕ_n and RR_n represent the angle and the R–R interval at time step n, respectively. It is deserved to note that testing for the angle map using surrogate data to preserve both the power spectrum and the histogram had been done in the work of Suder et al. (1998). In the following we will give different examples to illustrate the deterministic one-dimensional angle map can be derived under different situations.

2.6. Surrogate data analysis

The purpose of surrogate data is to test for any nonlinearity in the original data (Theiler et al., 1992). Surrogate signal is produced by phase randomizing the original data. It has similar spectral properties as of the given data. The surrogate data sequence has the same mean, the same variance, the same autocorrelation function and therefore the same power spectrum as the original sequence, but phase relations are destroyed. In the case of data shuffling, the histograms of the surrogate sequence and the reference sequence are identical. The random phase spectrum is generated by using the method of phase shuffle, where the phase values of the original spectrum are used in random order.

2.7. Mathematical model

In this study, we use the classic three-element Windkessel model (Westerhof et al., 1971) to simulate HRV, which describes the interaction between the cardiovascular system and baroreceptor control of arterial pressure. On the basis of the Windkessel theory, the dynamic relationship between the arterial pressure $P(t)$ and the cardiac output $Q(t)$ is

$$\frac{dP}{dt} - r\frac{dQ}{dt} = \frac{1}{RC}[(R+r)Q - P], \tag{3}$$

$$Q(t) = \frac{V_\tau(P)}{T_\tau(P)} = \frac{V(t-\tau)}{T(t-\tau)}, \tag{4}$$

where T and V mean, respectively, the period of the cardiac cycle and the stroke volume, and τ is the time delay in the human baroreceptor-mediated reflex. R, C, and r are, respectively, corresponding to a peripheral resistance, a total arterial compliance, and an aortic characteristic impedance. It is deserved to note that both T and V depend on the arterial pressure P. According to the sigmoidal law, $T(P)$ can be described as

$$T(P) = T_s + \frac{T_m - T_s}{1 + \gamma e^{-\alpha P/P_n}}, \tag{5}$$

where T_s and T_m establish the shorter and longer cardiac period and match, respectively, the maximal vasodepressor-induced sympathetic excitation and the maximal pressor-induced vagal activation (Franz, 1969). P_n corresponds to the steady level of arterial pressure. α and γ are two fitting parameters which determine range and slope of the linear region of the $T(P)$ curve. As for the stroke volume–pressure curve, the following expression is used.

$$V(P) = \frac{V_{max}}{1 + \beta\left(\frac{P}{P_v} - 1\right)^{-K}} \tag{6}$$

where β and K are fitting parameters, V_{max} is the maximum stroke volume, and P_v is the threshold for cardiac output. Table 1 illustrates the detailed parameter values used for numerical simulations. It shall be noted that the value of these parameters was estimated by best-fitting data drawn from physiological literature (Milnor, 1989; Korner et al., 1974).

Accompanying with the steady-state T–P as well as V–P curves, Eqs. (3) and (4) can be reduced to a delay-differential equation with one dynamical variable $P(t)$. By putting the obtained $P(t)$ into Eq. (5), then the period of the cardiac cycle is derived.

3. Results

3.1. Normal subjects

Fig. 1 illustrates time evolution of R–R intervals with/without nonlinear noise reduction. The *original* R–R intervals shown in the panel I of Fig. 1 are obtained from a healthy male voluntarily recorded under supine position. The recording process approximately lasts 2 h. It is obvious to see that this data exhibits low-frequency trend embedded in high-frequency fluctuations. Following the previous assumption of linear combination of a clean signal and a noise source, the *deterministic* R–R intervals can be derived after nonlinear noise reduction, which is shown in the panel III of Fig. 1. Evidently, high-frequency fluctuations are significantly reduced and the low-frequency variability is left. In particular, the histogram of high-frequency noisy fluctuations exhibits a symmetrical Gaussian-type distribution (Fig. 2). The underlying physiological process for noisy fluctuations can be revealed in terms of the well-known power spectrum analysis, from which it is quite straightforward to understand the contribution of noisy fluctuations being main from the respiratory band (see Section 4). Therefore, the variability of R–R intervals coming from RSA is treated as a stochastic source under our reduction scheme.

The associated angle maps corresponding to the R–R intervals shown in panels I and III of Fig. 1 are illustrated in panels II and IV of Fig. 1, respectively. In the recurrence plot of rotation angles for the *original* R–R intervals, it exhibits quite scattered behavior and does not show the deterministic one-dimensional structure

Table 1
List of parameters for model simulations

R	1.2×10^3 dyn s/cm^5	r	52 dyn s/cm^5	C	1.0×10^{-3} cm^5/dyn	P_n	89 mm Hg
P_v	25 mm Hg	T_s	0.66 s	T_m	1.2 s	V_{max}	86 cm^3
α	31	γ	6.7×10^{13}	β	72	K	7

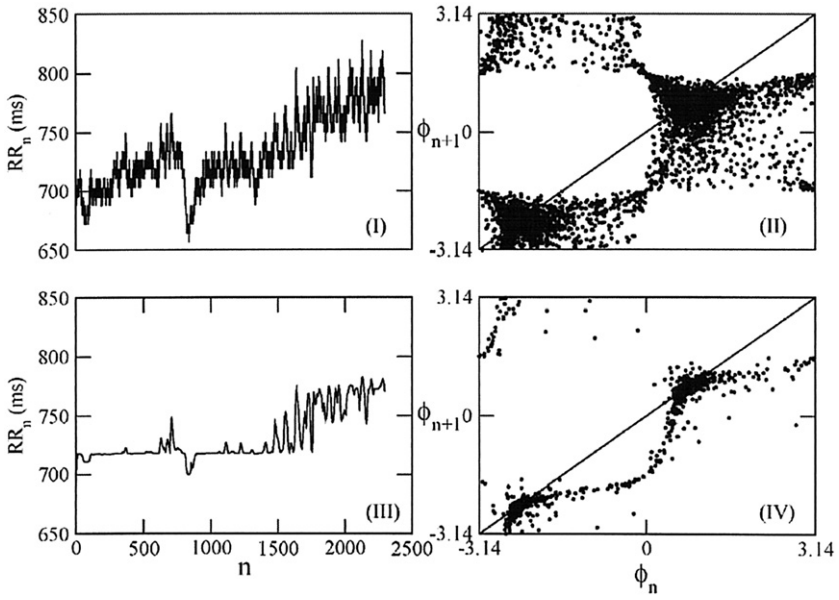

Fig. 1. Panels I and II denote the *original* R–R intervals and its corresponding angle map. Panels II and IV denote the *deterministic* R–R intervals and its corresponding angle map. Of particular note is that the recording process approximately lasts 2 h. In order to clearly visualize the variation of R–R intervals, only truncated heart beats are shown in panels I and III. But the angle maps shown in panels II and IV are derived from the complete R–R intervals.

(panel II). Nevertheless, the angle map for the *deterministic* R–R intervals displays a clear one-dimensional and well-harmonized nonlinear motion (panel IV). Of particular note is that the intersection points of the diagonal and the one-dimensional deterministic curve are located at $(\pi/4,\pi/4)$ and $(-3\pi/4,-3\pi/4)$. These points are corresponding to the fixed heart rate. The point $(\pi/4,\pi/4)$ is composed of three successive fixed R–R intervals which are larger than RR_a. In other words, three successive fixed R–R intervals, smaller than RR_a, are mapped to the point $(-3\pi/4, -3\pi/4)$. From the dynamical point of view, these two points can be realized as saddle points, from which "deterministic" HRV is regarded as intrinsically unstable.

3.2. ICU patients

Extracting the deterministic structure from noisy R–R intervals is of importance in fundamental research. Nevertheless, it is an interesting issue to test the nonlinear angle plot applied to risk stratification. So far, there is no consensus about the best available index of HRV for clinical use. Before we demonstrate the diagnostic results for ICU patients, we shall admit that using the dynamic characteristic of healthy individuals to predict the outcomes of ICU patients seems to violate the basic logic. However, this contradictory thinking contrarily inspires the different point of view compared to intuition. There is no doubt that there are two possible outcomes for ICU patients, in which one is transferred to

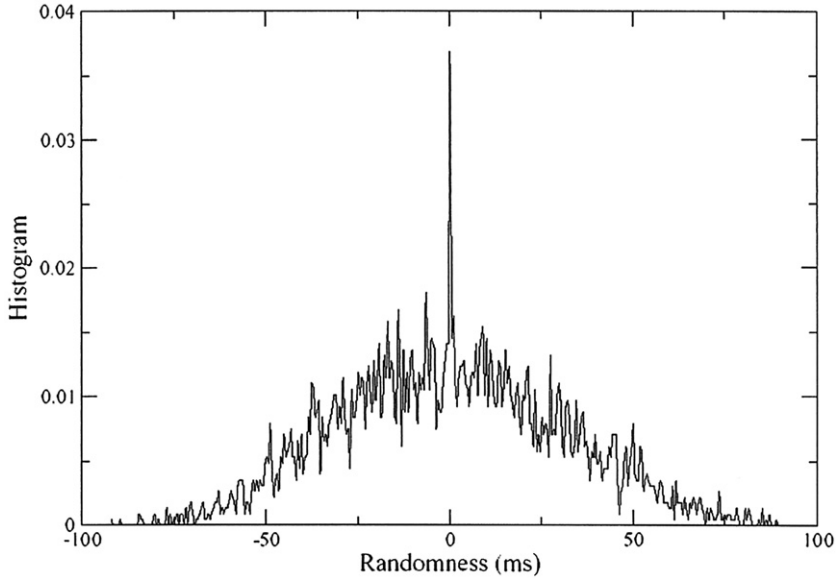

Fig. 2. The histogram of high-frequency noisy fluctuations is obtained from taking the difference of the *original* R–R intervals (panel I of Fig. 1) and the *deterministic* R–R intervals (panel III of Fig. 1).

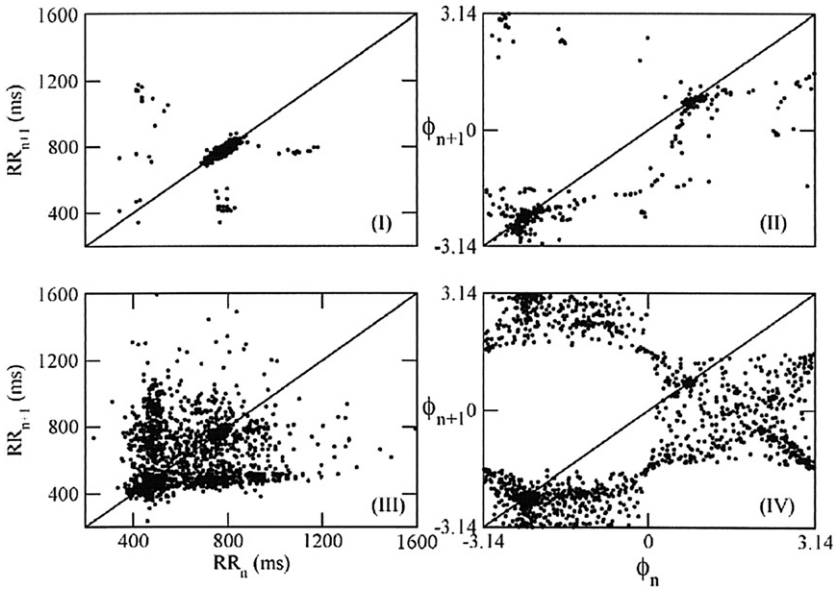

Fig. 3. Panels I and III denote two typical Poincaré plots for ICU patients. And the corresponding angle maps are shown in panels II and IV, respectively.

ordinary care units (OCUs) and the other is dying. The concept about OCU patients with stable signs of life seems reasonable, which definitely is the common point among healthy individuals. Therefore, using the dynamic characteristic of healthy individuals is to diagnose ICU patients with/without stable signs of life.

Fig. 3 provides two typical Poincaré plots for ICU patients. Panel I displays normal sinus rhythm with a compact elliptical structure exception of some ectopic heartbeats. In panel III it is evident to see that ectopic heartbeats are predominant and, further, the compact elliptical structure disappears and is replaced by the fanned out pattern. To state more clearly, homoclinic orbits can be directly observed in the panel III, which is known to be resulted from various types of pathological states, e.g., symptomatic sinus node dysfunction (Bergfeldt and Haga, 2003). After the process of noise reduction, the associated angle maps corresponding to panels I and III of Fig. 3 are illustrated in panels II and IV of Fig. 3, respectively. Panel II shows the deterministic one-dimensional structure analogous to that of healthy individuals, but in panel IV scattered points have a tendency to fill in the plane. Therefore, we may say that these two ICU patients have a distinct difference in mortality. Fig. 4 illustrates our dynamic risk stratification for ICU patients based upon the nonlinear map analysis. The last three days' ECG recordings of patient A are analyzed and shown in Fig. 4(a), where stable signs of life are clearly demonstrated during these days. Therefore, we diagnose patient A was transferred to OCU. Our diagnosis is right according to the hospital records. Fig. 4(b) is the analyzed outcomes of patient B according to the last seven days' ECG recordings. The three angle plots from 21 Aug. to 23 Aug. exhibit deterministic one-dimensional curves. Nevertheless, the last four days' angle plots are quite scattered, from which we judge patient B was dying. Our prediction is proved again by the hospital records. It is deserved to explain why patient B had a critical transition from 23 August to 24 August. According to historical records, medical doctor suspected that the unexpected leakage after surgery could be the main reason. Therefore, using angle maps to exactly predict the unexpected leakage seems nontrivial, moreover, intensive studies in other populations performed by independent investigators are definitely necessary in that topic. In addition to patients A and B, the outcomes of other 23 patients are also well described by the present method. In order to quantify the relation between Eq. (3) and angle plots obtained from ICU patients, we also calculate the cross correlation as a measure which is 0.73±0.13 for patients with stable signs of life (n=10) and, however, the other is 0.25±0.08 for critically ill patients (n=15),

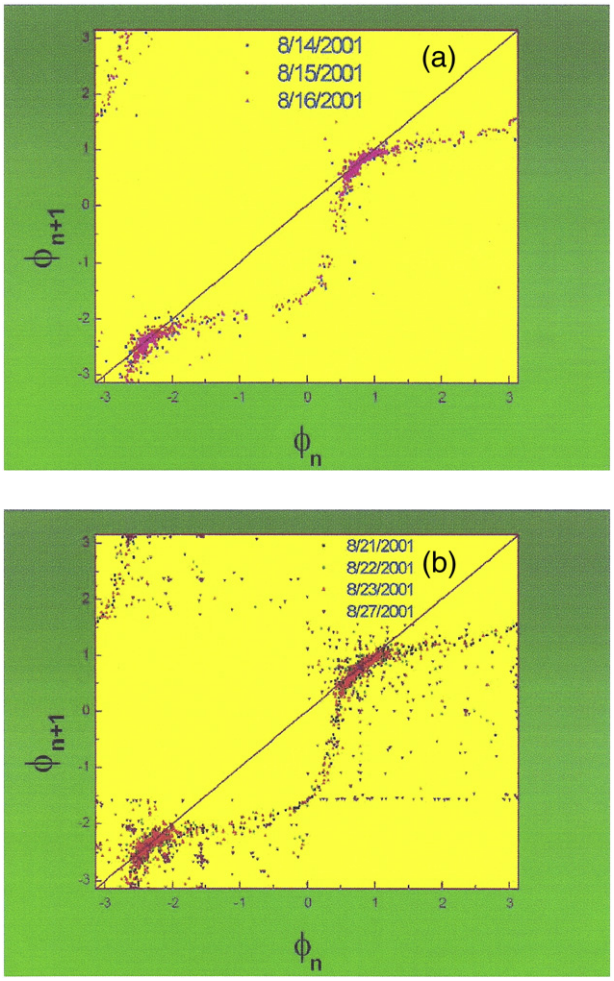

Fig. 4. The angle plot applied for the clinical diagnosis of two ICU patients, where different color symbols correspond to different measures. (a) It is evident to see the appearance of stable signs of life from patient A. Therefore, we judge this patient was transferred to OCU. (b) On the contrary, patient B lost stable signs of life, therefore, we judge this patient was dying. It shall be noted that the scattered points obtained from 24 August to 27 August have a tendency to fill in the plane. In order to clear visualization, we just show the data obtained from 27 August.

where the threshold separating the patient groups we used is 0.5. Therefore, there is a significant difference between these two possible outcomes of ICU patients. So far, it is known that a diagnosis of sepsis for ICU patients was associated with decreased total HRV, which strongly correlates with severity of illness (Garrard et al., 1993). However, in our study the degree of change in total HRV is not a good diagnostic index to describe illness severity of patient B. Thus, we might suggest that nonlinear map analysis on HRV applied to clinical utility could be promising. In order to give clear comparisons between different analyzed groups, the cross-correlation measure is listed in Table 2. Of particular note is that analyzing healthy subjects from the physionet public website are also included in Table 2 (www.physionet.org/physiobank/database). It is obvious to see that well-harmonized homeostasis still can be observed in this normal sinus rhythm R–R interval database.

3.3. Surrogate analysis

Surrogate analysis for the extracted deterministic data is performed and shown in Table 2, from which the extracted time series is statistically different from the surrogate. This rejects the null hypothesis and hence the fluctuations in the extracted time series have a deterministic/nonlinear structure. Moreover, surrogate analysis for the extracted noise is also performed in this study. The surrogate noise dataset was added to the extracted deterministic signal. Repeating the nonlinear noise-reduction procedure, we find that the new-generated deterministic signal behaves the same angle plot as the old one. According to this finding, the hypothesis on noise embedded in R–R intervals is further verified.

3.4. Model results

In these model simulations we only stress on the evolution of angle plots under the influence of time delay τ. When τ is smaller than 0.5 s, heart rate is not time dependent and the corresponding Poincaré plot shall exhibit a fixed point. The spontaneous heart rate fluctuations appear when τ is larger than 0.5 s, where τ=0.5 s is a threshold for occurring a supercritical Hopf bifurcation. In the range 0.5 s≤τ≤3 s the angle map displays the well-harmonized trajectory [Fig. 5(a)]. However, the well-harmonized profile will be gradually destructed due to the increase of τ values [Fig. 5(b)], and finally scattered points have a tendency to fill in the whole plane [Fig. 5(c)]. The basic reason for the angle plot shown in Fig. 5(c) is the appearance of spiky-like heart rate fluctuations when τ is large enough, which is a well-known phenomenon for delay-differential equations. Spiky fluctuations indicate fixed heart rate cannot be temporally assembled, thus scattered points in the angle plot cannot be accumulated at saddle points, i.e., (π/4,π/4) and (−3π/4,−3π/4). Instead, scattered points distribute in the whole plane. Compared to the map evolution of patient B shown in Fig. 4(b), we may say that the classic Windkessel model not only well describes why homeostasis can exist in heart rate fluctuations, but also provides a potential link between the clinical data and the circulatory system.

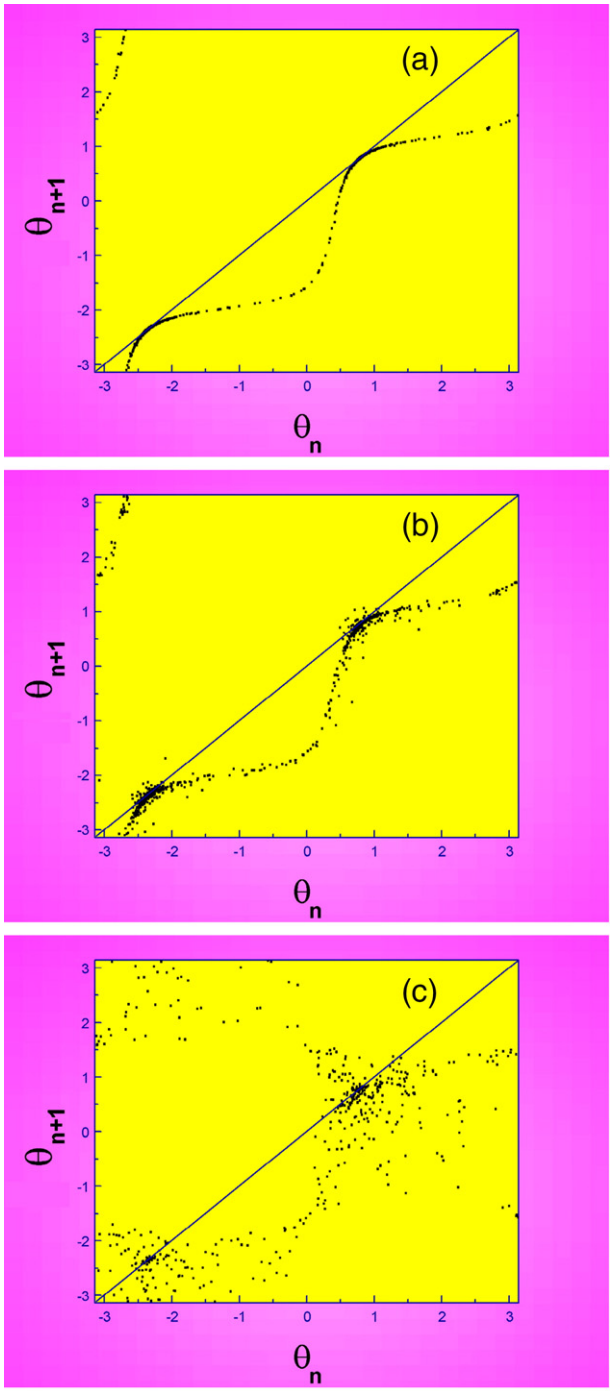

Fig. 5. Illustrations of the map evolution for different τ values. τ=(a) 2.5 s, (b) 3.2 s, and (c) 4.3 s. In order to discriminate angle maps derived from the clinical data or model simulations, θ_n is used to represent model results.

Table 2
List of cross-correlation measures for different analyzed groups

Data from Taipei Veterans General Hospital		
Healthy subjects	Male (n=15)	Female (n=10)
	0.75±0.12	0.74±0.15
	0.01±0.02[a]	−0.01±0.03[a]
ICU patients	Recovery (n=10)	Deterioration (n=15)
	0.73±0.13	0.25±0.08
	−0.03±0.04[a]	0.02±0.03[a]
Data from the physionet public website		
Healthy subjects	Male (n=15)	Female (n=13)
	0.71±0.11	0.72±0.13
	0.02±0.03[a]	0.01±0.03[a]

[a] Means results from surrogate data.

4. Discussions

Janson et al. (2001) introduced a model derived for the dynamics of angles of return times map of a periodic self-oscillatory system weakly forced by an arbitrary harmonic signal. The explicit map describing

the dynamics of angles for weak harmonic forcing is found to take the simple analytic form

$$\phi_n = \arctan(2\cos 2\pi\xi - \cot\phi_{n-1}) \quad (7)$$

where ξ is the rotation number, which is defined as the ratio of these two frequencies. If ξ tends to a very small values, this map equation can well describe the angle plot shown in the panel IV of Fig. 1. Therefore, based upon this theoretical model, we can further realize that the deterministic one-dimensional structure we obtained might be mainly resulted from the interaction of two independent frequencies, which could be explained via the function of autonomic nervous system on HRV, i.e., a kind of well-harmonized homeostasis. In addition, Eq. (7) can be extended as the limiting case resulting from a larger number of oscillators, where the oscillating frequencies are located in two different narrow bands. Owing to this concept, the appearance of a little bit noisy structure in the panel IV of Fig. 1 is expected.

The exhibition of autonomic nervous system can be traditionally realized via spectral analysis on HRV. In fact, interpretation of the spectrum itself is an active area of research. Usually the spectrum is broken into three regions for analysis. (a) The very low frequency (VLF) region covers from 0.000 to about 0.040 Hz. This region cannot usually be resolved but would be related with long-term factors such as thermoregulation of heart rate. (b) The low frequency range (LF, 0.040–0.150 Hz) often shows a peak at about 0.100 Hz, the origin of which is still unclear. Increased LF power may indicate sympathetic activation. (c) The high frequency region (HF, 0.150–0.400 Hz) covers rapid variations in heart rate due to vagal activity. In particular, human respiratory sinus arrhythmia is often seen between 0.180 and 0.400 Hz. And the central frequency for VLF, LF, and HF is corresponding to 0.003 Hz, 0.100 Hz, and 0.250 Hz, respectively. Table 3 illustrates linear measures, including SDNN as well as spectral analysis, for ICU patients. Obviously, most of these linear indices, exception of low-frequency power, are not good to identify the situations of ICU patients.

It is known that the spectral ratio LF/HF, i.e., the balance between sympathetic and vagal activities, was a classical homeostasis index for clinical diagnosis (Task Force of the European Society of Cardiology and the North American Society of Pacing and Electrophysiology, 1996). Nevertheless, Yien et al. (1997) clearly demonstrated that progressive increases in the power density values of both VLF and LF components appeared to be related to recovery for ICU patients. Conversely, progressive decreases in the power density values of these spectral components were indicative of deterioration and fatality. In the present study, the spectral power contributed by vagal tone is significantly reduced by using nonlinear noise-reduction method. The obtained deterministic one-dimensional angle map, in the point of view of autonomic tone, should be relevant to both VLF and LF. It is also deserved to note that the central-frequency ratio of VLF and LF is 0.03, which is close to the description by Eq. (7). To our best knowledge, it is little known that the correlation between VLF and LF could be a prognostic homeostasis index for ICU patients. In other words, our findings are quite different from the classical risk stratification (i.e., LF/HF) due to autonomic imbalance (Curtis and O'Keefe, 2002), and might be complementary to results reported by Yien et al.

Table 3
Results of SDNN and spectral analysis on ICU patients

ICU patients	Recovery ($n=10$)	Deterioration ($n=15$)	P value
SDNN (ms)	20.9±12.7	12.8±8.9	ns
LF (ms^2)	107.5±199.5	11.3±16.3	<0.05
HF (ms^2)	43.4±72.7	14.8±20.7	ns
LF/HF	2.9±1.9	2.3±3.2	ns
LF_n (nu)	68.5±13.2	50.7±23.7	ns
HF_n (nu)	31.2±14.2	48.3±24.7	ns

SDNN, standard deviation of the R–R intervals; LF, Low-frequency power; HF, high-frequency power; LF/HF, the ratio of Low-frequency to high-frequency power; LF_n, LF in normalized units; HF_n, HF in normalized units; and ns, no significance. All variables were obtained from 15-minute recordings and the level of statistical significance was set at $P<0.05$.

Concerning the classic Windkessel model, it is known that the spectral power mainly falls into both VLF and LF bands when a longer time delay is used to simulate (greater than 2 s). However, HF component will be dominant in the power spectrum for a shorter time delay (smaller than 1 s). Berger et al. (1989) estimated distinctly different delays in response to vagal or sympathetic stimulations, where vagal mediated changes begin almost immediately (≈0.6 s) and sympathetic mediated changes may begin after 1.7–2 s. Therefore, comparisons between Figs. 4(b) and 5 we may suggest that the correlation between VLF and LF plays a critical role to determine whether well-harmonized homeostasis exists in heart rate fluctuations.

Till to now, several authors have studied nonlinear measures in order to test their feasibility to identify changes in autonomic nervous system. In particular, Hagerman et al. disrupted the autonomic nervous activity to the heart with propranolol and atropine and found a reduction in the largest Lyapunov exponent (Hagerman et al., 1996). This confirms the potential value of using measures of nonlinear dynamics as a tool for evaluating autonomic nervous system to the heart. Interestingly, Hagerman et al. could not totally eliminate the nonlinear structures in HRV by using combined blockade. Thus they concluded that other mechanisms like circulating hormones, preload, or afterload contribute to the nonlinearity in HRV. Here, we give an example to address the underlying mechanisms of HRV could be beyond the only consideration of autonomic nervous activities. It is no doubt that the function of brainstem is strongly related to autonomic nervous activities. However, we analyzed R–R intervals of a little boy (4 years old) with brainstem dysfunction, and found the cross-correlation measure is around 0.81, which has no significant difference with those of normal subjects (see Table 1). This finding suggests that HRV could be from many factors rather than from autonomic nervous system, e.g., the classic Windkessel model. The detailed results of brainstem dysfunction will be published in elsewhere.

We would like to give more detailed remarks to address the possible difference between linear and nonlinear diagnoses. It is well known that linear SDNN method has a low accuracy for predicting the occurrence of life-threatening arrhythmias. What is the shortcoming of the SDNN method? We think it is a naturally born with problem. It is well accepted that cardiac dynamics is highly nonlinear. Bifurcations, chaos, and dynamical heterogenesis are all explored via experimental as well as theoretical studies in mammalian (Focus issue, 2002). A pronounced example of life-threatening arrhythmias is to consider ventricular tachycardia (VT), which is regarded as initiating abnormal/complicated spiral activities in ventricular tissue (Focus issue, 2002; Shiau et al., 2004). Intuitively, detecting spiral characteristics shall be analogous to HRV during VT period. These spirals are under the control of nonlinear evolution, therefore, the discovery of complexities buried in the nonlinear spiral could be beyond the capability of the linear method.

Finally, we would like to make our analyzed data available for analysis by other interested researchers. We wish that our data could be useful to the community of researchers.

5. Conclusions

Based upon the hypothesis of RSA fluctuations as a stochastic source, using the methods of noise reduction and angle map to extract the well-harmonized deterministic structure from R–R intervals is of great interest in both cardiac dynamics and nonlinear theory, where the concept of the interaction between different oscillators is suitable

to interpret our findings. Significant reduction of the contribution of the HF component, fixed heart rate is verified as intrinsically unstable, which could be influenced by both VLF and LF components. Particularly, the cross-correlation measure between the theoretical angle map and the numerically derived angle trajectory provides an additional non-invasive index in clinical research. Moreover, a simple physiologic model under the consideration of the influence of time delay in the human baroreceptor-mediated reflex is used to explain the clinical data. We wish that the discovery of well-harmonized homeostasis in heart rate fluctuations can raise more attractive studies in the future.

Acknowledgements

We really appreciate Dr. Sellier (Catania Univ., Italy) and Dr. Gong (Cornell Univ., USA) critically read the present manuscript and deliver encouraging comments. And we also thank for the research group of Dr. Yien (MD, Taipei Veterans General Hospital) providing HRV data This research was supported in part by the Institute of Physics, Academia Sinica, Taipei, Taiwan, the National Science Council, ROC, Grant No. NSC 93-2112-M-259-010, and Taipei Veterans General Hospital under Contract Nos. VGH 91-365-5.

References

Andrés, D.S., Irurzun, I.M., Mitelman, J., Mola, E.E., 2006. Increase in the embedding dimension in the heart rate variability associated with left ventricular abnormalities. Appl. Phys. Lett. 89, 144111.

Bergfeldt, L., Haga, Y., 2003. Power spectral and Poincaré plot characteristics in sinus node dysfunction. J. Appl. Physiol. 94, 2217–2224.

Balocchi, R., Menicucci, D., Santarcangelo, E., Sebastiani, L., Gemignani, A., Ghelarducci, B., Varanini, M., 2004. Deriving the respiratory sinus arrhythmia from the heartbeat time series using empirical mode decomposition. Chaos, Solitons Fractals 20, 171–177.

Berger, R.D., Akselrod, S., Gordon, D., Cohen, R.J., 1986. An efficient algorithm for spectral analysis of heart rate variability. IEEE Trans. Biomed. Eng. BME 33, 900–904.

Berger, R.D., Saul, J.P., Cohen, R.J., 1989. Transfer function analysis of autonomic regulation in canine atrial rate response. Amer. J. Physiol. 256, H142–H152.

Curtis, B.M., O'Keefe, J.H., 2002. Autonomic tone as a cardiovascular risk factor: the dangers of chronic fight or flight. Mayo. Clin. Proc. 77, 45–54 and references cited therein.

FOCUS ISSUE, 2002. Mapping and control of complex cardiac arrhythmias. Chaos 12, 732–981 and references cited therein.

Franz, G.N., 1969. Nonlinear rate sensitivity of the carotid sinus reflex as a consequence of static and dynamic nonlinearities in baroreceptor behavior. Ann. NY. Acad. Sci. 811–824.

Goldberger, A.L., 1996. Nonlinear dynamics for clinicians: chaos theory, fractals, and complexity at the bedside. Lancet 347, 1312–1314.

Goldberger, A.L., Rigney, D.R., West, B.J., 1990. Chaos, fractals and physiology. Sci. Am. 262, 42–49.

Goldberger, A.L., Mie, Tus Je., Rigney, D.R., Wood, M.I., Fortney, S.M., 1994. Effects of head-down bed rest on complex heart rate variability: response to LBNP testing. J. Appl. Physiol. 77, 2863–2869.

Garrard, C.S., Kontoyannis, D.A., Piepoli, M., 1993. Spectral analysis of heart rate variability in the sepsis syndrome. Clin. Auton. Res. 3, 5–13.

Huikuri, H.V., Seppanen, T., Koistinen, M.J., Airaksinen, K.E.J., Ikaheimo, M.J., Castellanos, A., Myerbutg, R.J., 1996. Abnormalities in beat-to-beat dynamics of heart rate before the spontaneous onset of life-threatening ventricular tachyarrhythmias in patients with prior myocardial infarction. Circulation 93, 1836–1844.

Hagerman, I., Berglund, M., Lorin, M., Nowak, J., Sylvén, C., 1996. Chaos-related deterministic regulation of heart rate variability in time and frequency domains: effects of autonomic blockade and exercise. Cardiovasc. Res. 31, 410–418.

Hegger, R., Kantz, H., 1999. Improved false nearest neighbor method to detect determinism in time series data. Phys. Rev. E 60, 4970–4973.

Ivanov, P.C., Amaral, L.A.N., Goldberger, A.L., Stanley, H.E., 1998. Stochastic feedback and the regulation of biological rhythms. Europhys. Lett. 43, 363–368.

Janson, N.B., Balanov, A.G., Anishchenko, V.S., McClintock, P.V.E., 2001. Modelling the dynamics of angles of human R–R intervals. Physiol. Meas. 22, 565–579.

Kantz, H., Schreiber, T., 1998. Human EGG: nonlinear deterministic versus stochastic aspects. IEE Proc.-Sci. Meas. Technol. 145, 279–284.

Kennel, M.B., Brown, R., Abarbanel, H.D.I., 1992. Determining embedding dimension for phase-space reconstruction using a geometrical construction. Phys. Rev. A 45, 3403–3411.

Korner, P.I., West, M.J., Shaw, J., Uther, J.B., 1974. Steady-state properties of baroreceptor heart rate reflex in essential hypertension in man. Clin. Exp. Pharmacol. Physiol. 1, 65–76.

Milnor, W.R., 1989. Hemodynamics. Williams & Wilkins, Baltimore.

Rosenblum, M., Kurths, J., 1995. A model of neural control of the heart rate. Physica A 215, 439–450.

Seidel, H., Herzel, H., 1998. Bifurcations in a nonlinear model of the baroreceptor–cardiac reflex. Physica D 115, 145–162.

Suder, K., Drepper, F.R., Schiek, M., Abel, H.H., 1998. One-dimensional, nonlinear determinism characterizes heart rate pattern during paced respiration. Am. J. Physiol. 275, H1092–H1102.

Schreiber, T., 1993. Extremely simple nonlinear noise-reduction method. Phys. Rev. E 47, 2401–2404.

Shiau, Y.H., Hsueh, M.P., Hseu, S.S., Yien, H.W., 2004. Complicated electrical activities in cardiac tissue. Int. J. Mod. Phys. B 18, 2645–2650.

Theiler, J., Eubank, S., Longtin, S., Galdrikian, B., Farmer, J., 1992. Testing for nonlinearity in time series: the method of surrogate data. Physca D 58, 77–94.

Task Force of the European Society of Cardiology and the North American Society of Pacing and Electrophysiology, 1996. Heart rate variability: standards of measurement, physiological interpretation, and clinical use. Circulation 93, 1043–1065 and references cited therein.

See Fig. 11(c) inWu, M.C., Huang, M.C., Yu, H.C., Chiang, T.C., 2006. Phase distribution and phase correlation of financial time series. Phys. Rev. E 73, 016118.

Westerhof, N., Elzinga, G., Sipkema, P., 1971. An artificial arterial system for pumping hearts. J. Appl. Physiol. 31, 776–781.

Yien, H.W., Hseu, S.S., Lee, L.C., Kuo, T.B.J., Lee, T.Y., Chan, S.H.H., 1997. Spectral analysis of systemic arterial pressure and heart rate signals as a prognostic tool for the prediction of patient outcome in the intensive care unit. Crit. Care Med. 25, 258–266.